https://doi.org/10.5194/egusphere-2025-2073
Preprint. Discussion started: 18 June 2025

Low-velocity and low-resistivity zone detected in the crust of the passive continental margin of south China

Shaoting Feng[1,2] Dikun Yang[1,2,3], Feng Jiang[4], Chunquan Yu[1,3], Xianglong Liu[1]

[1]Department of Earth and Space Sciences, Southern University of Science and Technology, China
[2]Southern Marine Science and Engineering Guangdong Laboratory (Zhuhai), Zhuhai, China
[3]Guangdong Provincial Key Laboratory of Geophysical High-resolution Imaging Technology, China
[4]South China Sea Institute of Oceanology, Chinese Academy of Sciences, China

Correspondence to: Dikun Yang (yangdikun@gmail.com)

Abstract. Passive continental margin has long been regarded as a tectonically and geo-dynamically inactive region with few discoveries of crustal unconformity and hence lacks scientific attention. However, previous seismic studies have hinted the presence of isolated crustal weak zones characterized by low shear-wave velocities in Guangdong-Hong Kong-Macao Greater Bay Area (GBA), north rim of South China Sea. In order to confirm the crustal heterogeneity, a 100 km-long magnetotelluric (MT) survey (ZHMT) was conducted across Zhuhai and Jiangmen (Guangdong Province) to fill in the blank of resistivity property in the region and to validate the crustal low-velocity zone at the research region. 3D inversion of the ZHMT data reveals a striking low-resistivity anomaly below the township of Shuangshui at the depth of 10-15 km depth. As plausible evidence of on-going or past tectonic activities, the Shuangshui Low-resistivity Anomaly (SLRA) is in a good spatial agreement with the low-velocity feature from the ambient seismic noise tomography. Two geological models are proposed for its origin: a fluid-bearing shear zone associated with deep faulting and fluid migration, or partial melting of mid-crustal material, possibly linked to anomalous heat flow. These findings provide new insights into the tectonic evolution of the passive margin at the research region, revealing previously unrecognized mid-crustal activity.

1 Introduction

The tectonic evolution of the South China Sea has profoundly influenced the geological framework and geodynamic processes along the southern margin of the Yangtze Craton, particularly within the Guangdong-Hong Kong-Macao Greater Bay Area (GBA) and the northern edge of the South China Sea. Despite its geological significance, this region has received considerably less attention than more tectonically active regions, such as the Himalayas. This is largely due to its classification as a passive margin—a term that conventionally implies tectonic quiescence and a well-understood geodynamic history (Buck, 2015). However, recent geophysical observations challenge this assumption.

Elevated surface heat flow (Kuang et al., 2021; Wang et al., 2022), widespread hot spring activity (Cai et al., 2024; Huang et al., 2022), and evidence of localized crustal deformation (Armitage et al., 2014; Pallister et al., 2010) suggest that the research region may not be as “passive” as traditionally thought. Similar findings have led researchers to reconsider the geodynamic

https://doi.org/10.5194/egusphere-2025-2073
Preprint. Discussion started: 18 June 2025

behaviour of passive margins worldwide. For instance, Ebinger and Belachew (2010), in their commentary on Pallister et al. (2010), proposed the concept of an "active passive margin" to describe regions where magmatic intrusions, fault reactivation, or anomalous heat flux indicate ongoing tectonic activity. Understanding the extent to which such processes operate in the region is critical not only for refining models of passive margin evolution but also for assessing regional geohazards and resource potential.

A major challenge in resolving these uncertainties is the lack of high-resolution geophysical data. The tectonic architecture of the region remains poorly constrained due to the scarcity of subsurface investigations, particularly in the electromagnetic domain, through which if a conductive zone is revealed, a more comprehensive conclusion on the presence of crustal weak zone can be drawn. To bridge this gap, we employ magnetotelluric (MT) methods to image the crustal electrical structure of the region. By integrating our findings with previous seismic studies, we aim to delineate crustal structures, identify potential geodynamic processes, and evaluate whether the research region exhibits characteristics of an 'active' passive margin.

1.1 Continental margin near the northern part of South China Sea

The continental margin near the northern part of South China Sea, situated at the southern margin of mainland China, represents a key economic and demographic centre recently known as the Guangdong-Hong Kong-Macao Greater Bay Area (GBA). GBA alone holds 9.5% of the entire population of China and over 10% of the entire GDP of China. The economic and urban expansion of the GBA is closely intertwined with its geological setting, which influences land use, resource distribution, and environmental hazards.

Despite its economic prominence, the region is susceptible to natural hazards, including earthquakes, landslides, and tsunamis. Although the region is generally considered seismically inactive, historical records indicate that massive earthquakes have occurred. The 1962 Xinfengjiang earthquake (Mw 6.1), induced by reservoir impoundment (Wu et al., 2024), resulted in 10 fatalities and extensive damage to local housing. More recently, the 1994 Beibu Gulf earthquake (Mw 6.1) caused one fatality and injured over 600 people, while a similar event in 1995 led to hundreds of additional injuries. In the past five years, an increasing number of small earthquakes (Mw 3-4 with an epicentre depth around 10 km) have been recorded in the region (Bao et al., 2024; Huang et al., 2023; Kang et al., 2008), though they have received less public and scientific attention. This aligns with Ebinger's observation that "active passive margins" often experience micro-seismicity below the detection threshold of global seismic networks. These occurrences suggest that, despite the region's classification as a passive margin, stress accumulation and fault reactivation may still play an active role, warranting further geophysical investigation.

A key structural feature in this region is the Littoral Fault Zone (LFZ), a major fault system situated on the continental shelf of the South China Sea, running parallel to the South China coastline (Zhang et al., 2004). While the LFZ itself does not extend onshore, its deep structure may have significant implications for the onshore crustal architecture. Offshore investigations have provided insights into its characteristics, but how its tectonic influence propagates inland remains poorly constrained due to

https://doi.org/10.5194/egusphere-2025-2073
Preprint. Discussion started: 18 June 2025

limited geophysical data. Given the region's dense population and economic significance, resolving the extent to which the LFZ affects regional crustal deformation is crucial for hazard assessment and geodynamic modelling.

Additionally, the region exhibits above-average surface heat flow, a high density of hot springs, and other geophysical anomalies that raise questions about the extent to which this region conforms to the traditional model of a passive margin. Investigating these features in greater detail will help clarify the role of deep-seated tectonic and magmatic processes in shaping the regions' evolution.

1.2 Previous Studies in the region

Geophysical studies in the research region remain limited due to intense human activity, strong electromagnetic interference, and the logistical challenges of conducting field surveys in highly developed areas. However, several key studies have provided valuable insights into the regional's tectonic framework.

Seismic Imaging and Crustal Velocity Models

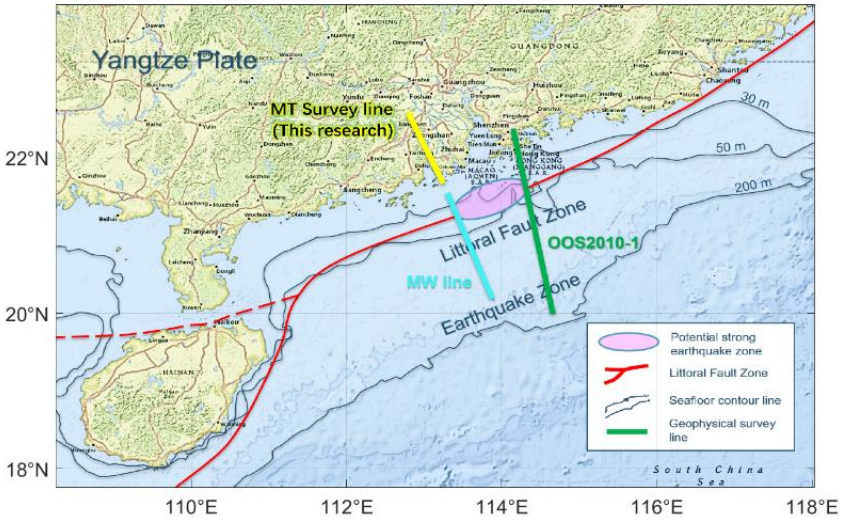

Figure 1: The corresponding survey lines: MW seismic survey line (Xiong et al., 2018) in cyan colour, OOS2010-1 offshore seismic survey line (Cao at el., 2014) in green colour, and the ZHMT survey line of this research in yellow colour. (Basemap source: Esri)

By integrating multi-channel seismic reflection data with P-wave velocity models derived from seismic ray tracing, Cao et al. (2014) and Xiong et al. (2018) constructed two 2D velocity models along the MW and OOS2010-1 profiles respectively. These models extend to approximately 30 km depth, capturing the transition from the upper crust to the Moho. The seismic results reveal a layered crustal structure with increasing velocity at depth, consistent with typical continental margins. Notably, the velocity model along the OOS2010-1 profiles identifies a distinct low-velocity zone at 15-20 km depth on the eastern side of the Pearl River Delta. This anomaly gradually thins as it approaches the offshore region. However, due to the limited station

https://doi.org/10.5194/egusphere-2025-2073
Preprint. Discussion started: 18 June 2025

distribution and relatively short offsets in Xiong's dataset, a similar low-velocity structure has not been detected on the western side of the Pearl River Delta.

Further inland, Lü et al. (2022) conducted a more extensive seismic survey on behalf of the Guangdong Earthquake Agency. Using ambient noise tomography and surface wave inversion techniques, they generated a 3D shear-wave velocity model of the region. While their primary focus was on fault structures within the upper 10 km of the crust, re-plotting the S-wave velocity profile along the landward extension of the MW survey line reveals a localized decrease in velocity at approximately 10 km depth and beyond (Fig.2 (a)). This feature may correspond to previously observed low-velocity anomalies, though further validation is required.

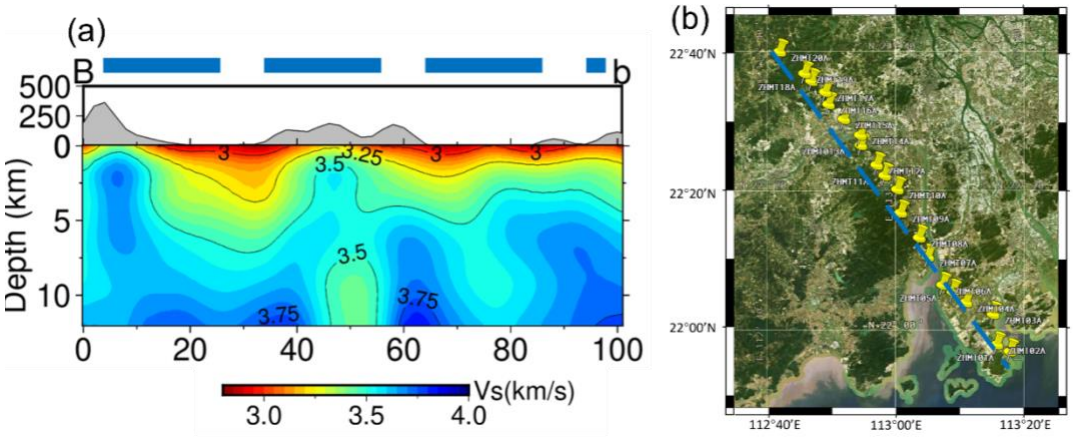

Figure 2: Shear-wave velocity model in the research region. (a) The S wave velocity model of landward extension of the survey line MW which aligns with the ZHMT survey line of this research (Lü et al., 2022), with the capitalized letter 'B' representing the northwesternmost station and 'b' representing the southeasternmost station. (b) The detailed locations of survey line: the yellow pins represent the survey stations of ZHMT (satellite image source: Google Earth Pro, © Google).

Implications for Crustal Weak Zones

The presence of low-velocity zones at the passive margin transition from continental to oceanic crust, such as along the South China coastline, can arise from a range of geological processes. Cao et al. (2014) proposed that the low-velocity anomaly beneath the OOS2010-1 line results from partial melting of hydrated crustal material, marking a transition from brittle to more ductile deformation. Given its relatively low strength, such a weak zone could also facilitate crustal stress transfer, potentially influencing regional fault activity.

From a geophysical perspective, low-velocity zones are often associated with low-resistivity anomalies, as increased water content reduces both seismic velocity and electrical resistivity (Meju et al., 2003; Moorkamp et al., 2013). This relationship provides a valuable resistivity constraint on suspected tectonic activities in the crust. In this research, we employ Magnetotelluric (MT) methods to complement previous seismic investigations, aiming to better characterize the electrical structure of the research region and refine our understanding of regional crustal weak zones.

https://doi.org/10.5194/egusphere-2025-2073
Preprint. Discussion started: 18 June 2025

2 Method

Magnetotelluric (MT) surveying, a passive-source electromagnetic method, was employed to investigate the subsurface electrical structure of the continental margin near the northern part of the South China Sea. This technique measures natural variations in the Earth's electric and magnetic fields across a wide frequency spectrum to infer subsurface resistivity distribution. MT is particularly effective in detecting variations in conductivity associated with geological structures such as fluid-bearing fault zones, partially molten regions, and lithological boundaries. However, its sensitivity to electromagnetic noise necessitates careful data processing, particularly in regions with significant human activity.

The implementation of MT in the research region presented challenges due to the region's dense infrastructure and industrial activities, which contribute to strong electromagnetic interference. To mitigate these effects, we optimized station locations to minimize anthropogenic noise while ensuring comprehensive spatial coverage. The survey design also incorporated robust data processing techniques to enhance signal quality and improve inversion reliability.

2.1 MT Survey Configuration

To validate and extend previous seismic findings, we designed our MT survey line to align with the MW seismic profile (Xiong et al., 2018) and extended it landward to cover key areas including Zhuhai, Jiangmen, and Heshan.

The MT survey line spans 100 km, following a trajectory semi-perpendicular to the coastline of South China. A total of 20 original stations and 2 supplementary stations were deployed, with an average station spacing of 5 km (Fig.2 (b)). The line traverses Jinwan (Zhuhai), Xinhui (Jiangmen), and Heshan (Jiangmen), targeting regions with minimal anthropogenic interference.

Despite efforts to select remote locations, certain areas still exhibited significant electromagnetic noise. In Jinwan, widespread aquaculture activities—including aeration systems in densely packed fishponds—introduced persistent noise. Similarly, in Xinhui, small-scale industrial facilities with irregular operating schedules contributed to unpredictable interference. These factors necessitated careful noise filtering during data processing.

At each site, two orthogonal electrode pairs were buried in soil to measure the electric field in the north-south (Ex) and east-west (Ey) directions, with an average electrode spacing of 50 meters. This configuration balances the need for sufficient signal sensitivity while accommodating field constraints. Magnetic field measurements were obtained using three orthogonally positioned coil sensors: Hx (north-south), Hy (east-west), and Hz (vertical).

Data acquisition at each station lasted for at least 60 hours, using the Phoenix MTU-5A system. To capture a broad frequency range, the system recorded at a 15 Hz sampling rate continuously, supplemented by 150 Hz and 2400 Hz bursts collected every 10 minutes for high-frequency resolution.

https://doi.org/10.5194/egusphere-2025-2073
Preprint. Discussion started: 18 June 2025

2.2 Data Processing

The acquired MT data underwent rigorous processing to enhance signal quality and extract reliable impedance estimates for inversion. Given the survey's proximity to urbanized and industrial areas, mitigating the effects of electromagnetic noise was a primary challenge. Data processing followed a structured approach, including time-domain analysis, frequency-domain filtering, and data selection based on spectral characteristics. The MTDP software package (Wang et al., 2024) was employed for robust data screening and processing.

Noise sources in the study area were diverse and included: power line interference at 50 Hz and harmonics; industrial machinery and aquaculture operations, generating broadband noise; and irregular transient signals, likely from intermittent electrical discharges. To address these challenges, we applied a combination of statistical noise rejection, remote reference processing, and frequency-domain filtering to improve data fidelity before inversion.

2.2.1 Time-domain Analysis

Time-series analysis was conducted to assess data quality and identify non-stationary noise sources. Initial visualization of raw time-series data revealed significant site-to-site variations in signal integrity, with urban-proximal stations exhibiting higher levels of anthropogenic interference.

Particularly strong noise contamination was observed at stations ZHMT04A to ZHMT07A, located near the mouth of the Pearl Rivere Delta. These stations exhibited persistent, high-amplitude disturbances, likely related to extensive reclamation activities and aquacultural infrastructure in the estuary. Fourier analysis using a Hann window and 2048-sample segments revealed unexpected spectral peaks at 20 Hz and 26 Hz (ZHMT04A) and 15 Hz and 33 Hz (ZHMT06A), indicating local electromagnetic interference sources. At ZHMT05A, a more complex noise signature was detected, with multiple spectral peaks spanning 15 Hz to 40 Hz, suggesting multiple overlapping interference sources.

Beyond periodic disturbances, irregular transient noise was also identified in several stations. These transient signals, characterized by sudden amplitude spikes followed by gradual decay, resembled impulse responses and were not clearly identifiable in frequency-domain spectra. Such events, likely linked to intermittent industrial activity or sporadic electrical discharges, posed additional challenges for standard filtering techniques.

To mitigate these issues, we applied 1) windowed statistical filtering, excluding extreme amplitude outliers from further processing and 2) remote reference correction, using the remote station in Sichuan to suppress correlated noise. These preprocessing steps improved data quality, ensuring that meaningful geophysical signals were retained for subsequent impedance estimations.

https://doi.org/10.5194/egusphere-2025-2073
Preprint. Discussion started: 18 June 2025

2.2.2 Data selection and Rho plus model

Given the significant electromagnetic interference in the area, a systematic data selection process was implemented to ensure that only high-quality data were used for inversion. This process involved evaluating multiple criteria, including phase coherence, spectral density, polarization characteristics, and signal-to-noise ratio (SNR). The MTDP software package (Wang et al., 2024) was used to implement robust filtering and selection strategies.

Phase and Spectral Density Screening

Initially, phase consistency was examined to exclude unreliable data points. Data were considered valid if phase angles fell within the expected range from 0° to 90° for Zxy and from -90° to -180° for Zyx. Any phase values outside these ranges were discarded, as they often resulted from strong near-field interference or poorly constrained impedance estimates.

Next, spectral density analysis was performed to differentiate true MT signals from anomalous noise spikes. Data points with spectral densities exceeding two or three orders of magnitude above the regional average were classified as outliers and removed.

Polarization and Coherence Filtering

Polarization analysis was used to assess whether the electric and magnetic fields exhibited expected natural-source behaviour. Data showing excessive clustering along specific polarization angles were flagged as potential noise-contaminated records.

Coherence analysis was also applied, comparing signal similarity between the main stations and the remote reference station. Data with extremely low coherence values (indicating uncorrelated local noise) or excessive high coherence (suggesting persistent artificial sources) were removed from further processing.

Implementation of the Rho-plus Model

To further refine the dataset, the Rho-plus model was employed as a consistency check. The Rho-plus model generates a theoretical apparent resistivity curve based on physically constrained assumptions, along for an iterative comparison between observed and modelled data.

The data selection process was refined through iterative cycles:

1. Initial impedance computation to generate raw apparent resistivity curves.
2. Comparison with the Rho-plus model to detect significant deviations.
3. Progressive filtering of outliers, followed by model recalibration.

This iterative approach ensured that the final dataset was both geophysically plausible and minimally affected by anthropogenic noise, improving the robustness of the subsequent inversion process.

https://doi.org/10.5194/egusphere-2025-2073
Preprint. Discussion started: 18 June 2025

2.2.3 Impedance estimation and analysis

Following time-domain preprocessing and data selection process in both time domain and frequency domain, the screened MT dataset was used to compute impedance tensors, phase tensors, and geomagnetic transfer functions. These parameters provide critical information about subsurface resistivity variations and structural anisotropy.

Impedance Tensor Calculation

The impedance tensor (Z) was computed using the relation:

$$\begin{bmatrix} E_x \\ E_y \end{bmatrix} = \begin{bmatrix} Z_{xx} & Z_{xy} \\ Z_{yx} & Z_{yy} \end{bmatrix} \begin{bmatrix} H_x \\ H_y \end{bmatrix} \quad (1)$$

Where E_x, E_y are the measured electric fields, and H_x, H_y are the magnetic field components. The diagonal elements (Z_{xx}, Z_{yy}) ideally approach zero in 2D structures, while the off-diagonal terms (Z_{xy}, Z_{yx}) contain resistivity and phase information.

To minimize bias from noise-contaminated data points, impedance estimates were refined using robust regression techniques. High-leverage outliers, often introduced by anthropogenic interference, were down-weighted to improve stability. Additionally, remote reference processing was applied where coherence with the reference station exceeded 0.6, enhancing signal fidelity at lower frequencies.

Phase Tensor Analysis and Dimensionality Assessment

To evaluate structural dimensionality, phase tensor (Φ) were derived from impedance data through eigenvalue decomposition:

$$\Phi = Im(Z)Re(Z)^{-1} \quad (2)$$

Where $Im(Z)$ and $Re(Z)$ represent the imaginary and real components of the impedance tensor, respectively.

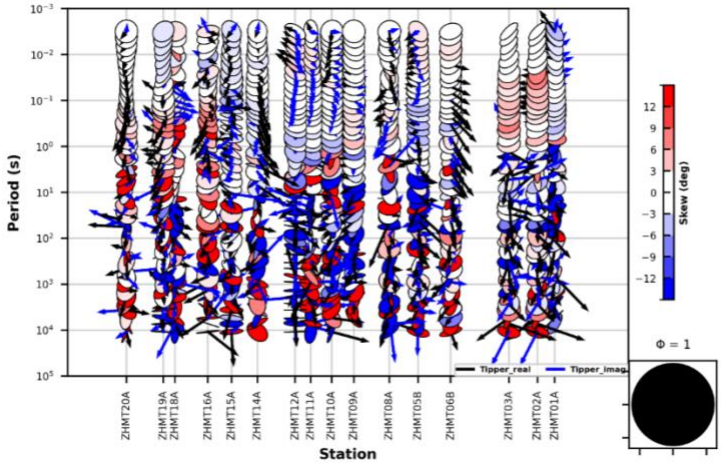

Figure 3: The phase tensor and tipper (black arrow as real part, blue arrow as imaginary part) of the raw data along the MT survey line.

https://doi.org/10.5194/egusphere-2025-2073
Preprint. Discussion started: 18 June 2025

MTpy (Kirkby et al., 2019) was used to plot phase tensor ellipses and geomagnetic tippers along the survey line in Figure 3 as a qualitative interpretation of the field data. At shallow depths (periods 0.001 s to 1 s), skew angles remain within ±3°, suggesting a predominantly 1D or 2D resistivity structure. However, at longer periods (> 1 s), skew angles increase, indicating a more complex 3D conductivity distribution at greater depths; the data quality also deteriorates significantly, because the long-period signals are usually much weaker compared to the noise at the same frequencies.

Geomagnetic Transfer Function Analysis: Tipper

The geomagnetic transfer function, represented by the tipper (T), was computed as:

$$T = \frac{H_z}{H_x^2+H_y^2} \quad (3)$$

Where H_z is the vertical magnetic field component. The tipper provides additional constraints on lateral conductivity contrasts. As shown in Figure 3, tipper orientations remain relatively consistent at short periods, suggesting laterally uniform conductivity at shallow depths. Notably, stations ZHMT02A and ZHMT03A exhibit strong anisotropy, suggesting localized heterogeneity even at shallow depths. However, at longer periods, the tipper data are strongly affected by the local interference and present irregular variations.

The combination of phase tensor analysis and tipper data suggests that shallow crustal conductivity is relatively uniform, while deeper structures exhibit significant lateral variations.

Apparent Resistivity and Phase Analysis

The apparent resistivity and impedance phase were computed based on the impedance tensor using the following expressions:

$$\rho_{ij} = \frac{|Z_{ij}(\omega)|^2}{\omega\mu_0} \quad i,j \in x,y\,, \quad (4)$$

$$\varphi_{ij} = \tan^{-1}\frac{Im(Z_{ij})}{Re(Z_{ij})} \quad i,j \in x,y\,, \quad (5)$$

where ρ represents the apparent resistivity, Z represents the impedance, ω represents the angular frequency of the electromagnetic field, μ_0 as the permeability of free space; φ as the phase, $Im(Z)$ as the imaginary part of impedance, and $Re(Z)$ as the real part of impedance. The subscripts i,j are used to annotate the order of the computation of the complex number Z which has four directions including Z_{xx}, Z_{xy}, Z_{yx}, and Z_{yy}.

Most of the apparent resistivity curves exhibit steep inclinations at high frequencies, likely influenced by near-field electromagnetic interference from anthropogenic sources such as power lines, industrial activity, and aquaculture systems. Additionally, signal complexity at low frequencies suggests that long-period data have also been affected by regional noise sources, making robust processing essential.

https://doi.org/10.5194/egusphere-2025-2073
Preprint. Discussion started: 18 June 2025

Despite these challenges, the apparent resistivity curves exhibit generally continuous and smooth variations between 300 Hz and 1 s, closely resembling the trends observed in phase tensor plots. This continuity suggests that data within this frequency range maintain a stable signal-to-noise ratio, making them suitable for further inversion and interpretation.

To facilitate visualization and assess large-scale resistivity variations, a pseudo-section of apparent resistivity and phase angle was generated, as shown in Figure 4.

A notable decrease in resistivity is observed in the in-land section of the profile, approximately one-quarter from the left, corresponding geographically to Xinhui, Jiangmen. The phase pseudo-section further corroborates this anomaly, showing a distinct low-resistivity feature between 0.1 s and 1 s at the same location, suggesting a significant conductivity contrast at mid-crustal depths.

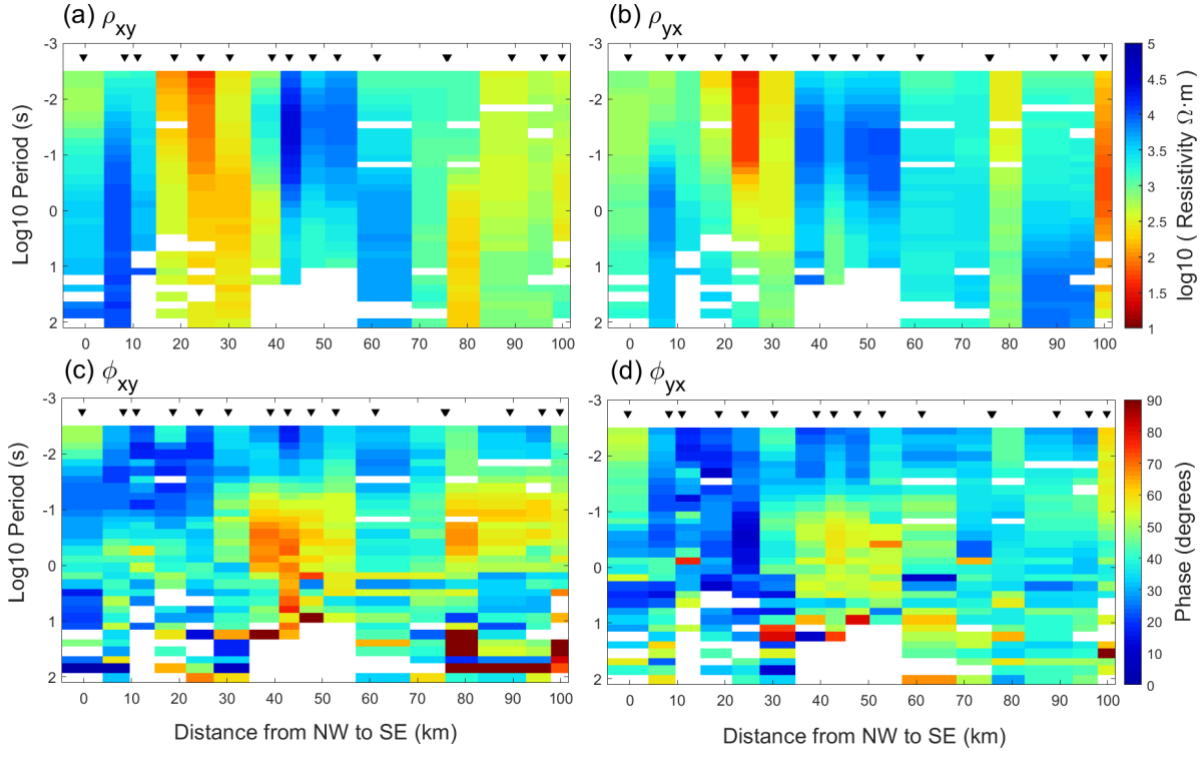

Figure 4: The pseudo-section of the raw data along the MT survey line. (a) and (b) represent apparent resistivity in the XY and YX polarization modes, while (c) and (d) represent the phase responses in the same respective directions.

These observations provide crucial preliminary constrains on subsurface resistivity distribution and serve as key assessment criteria for the subsequent inversion process.

https://doi.org/10.5194/egusphere-2025-2073
Preprint. Discussion started: 18 June 2025

2.3 Inversion

Inversions are often necessary to derive a subsurface resistivity model from the processed Magnetotelluric (MT) data. Although our dataset was acquired along a single line, we still prefer a 3D inversion to fully accommodate any possible 3D structure indicated in the qualitative analyses. Particularly, we employed the ModEM inversion framework (Kelbert et al., 2014), a widely used 3D inversion algorithm based on the finite difference modelling and nonlinear conjugate gradient (NLCG) minimization method. ModEM recovers the subsurface resistivity distribution by iteratively minimizing the misfit between observed and predicted impedance responses. The inversion is regularized using smoothness constraints to stabilize the solution while preserving geologically meaningful resistivity contrasts.

The inversion minimizes the objective function:

$$\Phi = \sum_i \left(\frac{d_i^{obs} - d_i^{cal}}{\sigma_i} \right)^2 + \lambda R(m) , \quad (6)$$

where d_i^{obs} and d_i^{cal} represent the observed and calculated data, respectively; σ_i is the data uncertainty; $R(m)$ is the regularization term enforcing spatial smoothness, and λ is the regularization parameter balancing data misfit and model smoothness.

To initiate the inversion, we constructed a 3D resistivity mesh covering the survey region. The initial model was set as a homogeneous half-space with a resistivity of 100 Ω·m. The core of the model consists of a centre mesh with 2 km spacing in both the North-South and East-West directions, extending approximately 80 km along the E-W direction and 100 km along the N-S direction to encompass the MT survey line. To minimize boundary effects, eight padding cells were added in both the N-S and E-W directions, expanding outward by a factor of 1.3. Vertically, the first layer was assigned a thickness of 100 m, with subsequent layers increasing in thickness by the same 1.3 factor to ensure adequate resolution at depth.

Sixteen out of the 22 surveyed stations (ZHMT01A-03A, ZHMT05B, ZHMT06B, ZHMT09A-12A, ZHMT14A-16A, ZHMT18A-20A) were incorporated into the inversion, with data frequencies extending up to 10 seconds across a total of 31 frequency points. A 5% relative error threshold was imposed to ensure stability, yielding a final misfit of 1.3, indicating a reasonably converged solution.

Cross-section along the ZHMT survey line is sliced from the final inverted resistivity model (Fig.5) to analyse the sub-surface features beneath the survey stations.

https://doi.org/10.5194/egusphere-2025-2073
Preprint. Discussion started: 18 June 2025

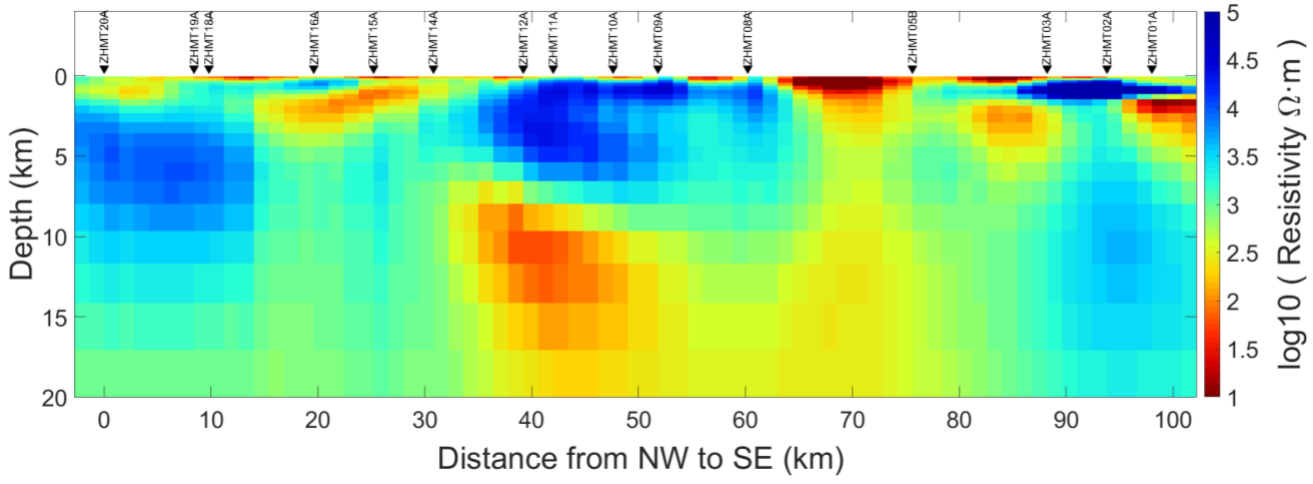

290 **Figure 5: Cross section of the resistivity model along the MT survey line.**

2.3.1 Verification of low-resistivity anomaly

To ensure the reliability of the inverted resistivity model, we conducted forward modelling tests to verify the presence of a significant low-resistivity anomaly identified at depths of 10-15 km beneath stations ZHMT11A and ZHMT12A at Xinhui.
295 The verification process involved modifying the resistivity model to assess the impact of the anomaly on surface responses. First, a control model was generated by replacing the low-resistivity anomaly with a homogeneous resistivity of 100 Ω·m, matching the background resistivity of the surrounding crust. This modification allowed us to compare the predicted response of a model without the conductive anomaly against the original field data.

Using this modified model, forward responses were computed over the same frequency range as the observed data (300 Hz to
300 0.1 Hz), ensuring that the sensitivity to deep structures was adequately tested. The key diagnostic parameters examined included apparent resistivity curves and phase angle responses at affected stations.

305

310

https://doi.org/10.5194/egusphere-2025-2073
Preprint. Discussion started: 18 June 2025

Comparison of Forward Responses and Field Data

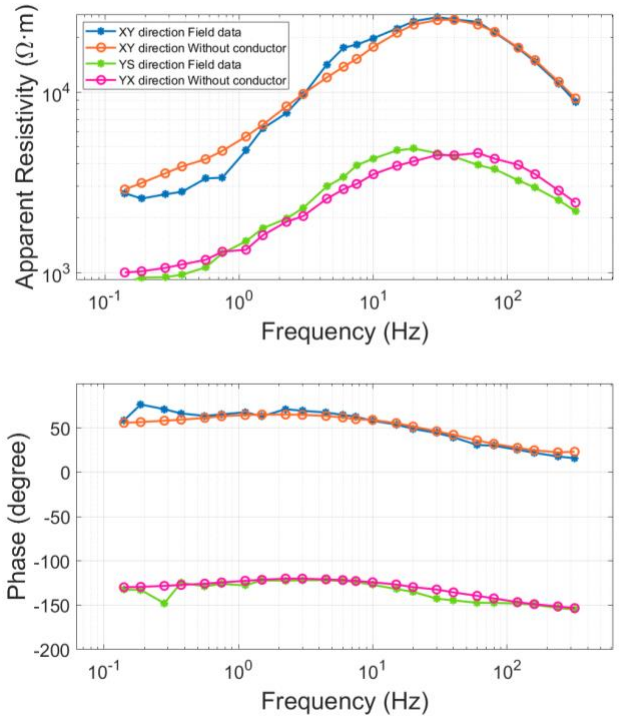

Figure 6: The comparison of apparent resistivity and phases curves between the field data and forward responses of anomaly-removed model at the station of ZHMT11A.

The comparison reveals that at lower frequencies (longer periods, deeper penetration), the observed field data exhibit lower apparent resistivity values and higher phase angles compared to the forward model without the anomaly; removing the conductive structure increases the apparent resistivity and reduces the phase shift, indicating that the original inversion correctly captured a real, conductive feature at depth (Figure 6).

These results confirm that the presence of the low-resistivity anomaly in the crust is not an inversion artifact, but a necessary feature required to reproduce the observed MT responses. The strong conductivity contrast suggests either fluid enrichment or a deep-seated weak zone, warranting further geological interpretation in subsequent sections.

2.3.2 Consideration of ocean and sediment effects in inversion

Given the proximity of the MT survey to the coastline of the South China Sea, the potential influence of conductive seawater and thick sedimentary deposits on inversion results must be carefully considered. The presence of a highly conductive ocean can introduce static shifts and distort subsurface resistivity estimations, particularly for shallow and intermediate depths.

https://doi.org/10.5194/egusphere-2025-2073
Preprint. Discussion started: 18 June 2025

Similarly, low-resistivity sediments near estuarine regions can affect the measured impedance tensors, potentially leading to misinterpretation of deeper structures.

To assess these effects, we incorporated coastline geometry and regional sediment distribution into the inversion mesh. The ocean was assigned a uniform resistivity of 0.3 Ω·m. representative of seawater conductivity, while nearshore sedimentary layers were constrained based on prior geological and seismic studies. This modification aimed to reduce boundary artifacts and ensure a more realistic resistivity distribution in the inversion model.

Impact of Ocean and Sediments on Resistivity Models

To quantify the influence of these conductive layers, we performed a comparative analysis using two initial models:

1. A half-space model with no explicit ocean or sediment constraints.
2. A coastline-constrained model, where the ocean and sediment layers were predefined with fixed resistivity values.

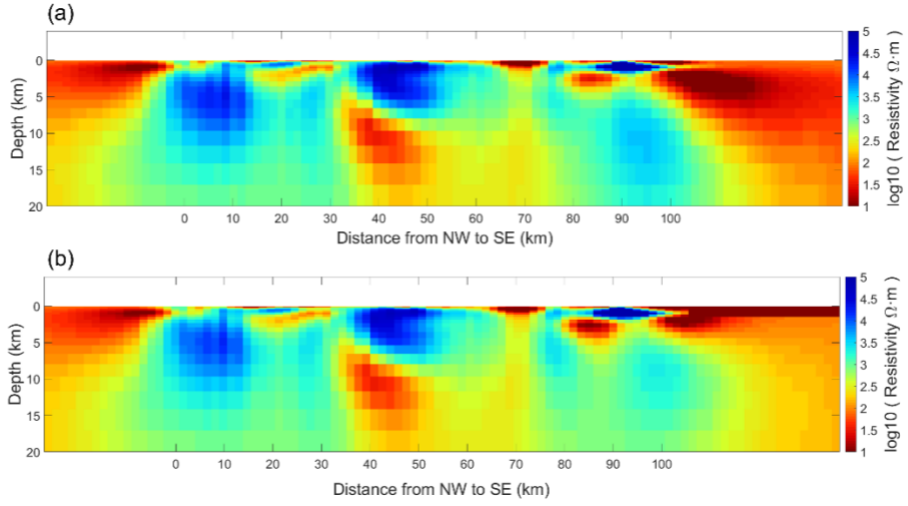

Figure 7: The resistivity model comparison between initial model of (a) half space and (b) of ocean and sediment layer fixed.

Figure 7 presents the resistivity models generated from these two setups. The comparison indicates that in the half-space model, resistivity variations near coastal stations appear exaggerated, suggesting that the inversion attempted to compensate for the unmodeled ocean effect. In the coastline-constrained model, resistivity distributions appear more geologically reasonable, with smoother transitions between land and sea regions. The deep crustal structures remain largely unaffected, confirming that the primary anomalies in the final model are robust and not artifacts introduced by coastal effects.

These results indicate that while the ocean and sediments exert some influence on shallow and mid-crustal resistivity patterns, their impact on deeper structures is minimal. By incorporating realistic conductivity constraints into the inversion, we ensured that the final resistivity model more accurately reflects true subsurface conditions.

https://doi.org/10.5194/egusphere-2025-2073
Preprint. Discussion started: 18 June 2025

3 Results and discussion

The inverted resistivity model provides new insights into the crustal structure of the research region, revealing distinct conductivity variations that correlate with known geological features and potential deep-seated anomalies. To ensure the reliability of these findings, extensive verification procedures, including forward modelling and sensitivity tests, were conducted to distinguish true geophysical signals from inversion artifacts. The results not only align with existing seismic studies but also highlight previously unrecognised structures that may have significant geodynamic implications.

This section presents a comprehensive analysis of the results, structured as follows:

1. Electromagnetic environment assessment—examining effects of noise sources on data quality and ensuring the validity of the inversion outcomes.
2. Resistivity model interpretation—identifying key conductive and resistive structures and discussing their geological significance.
3. Geological and tectonic implications—integrating these findings with existing geophysical data to assess the broader implications for passive margin evolution and regional geodynamics.

Through this analysis, we aim to refine the understanding of crustal conductivity variations in the research region and evaluate whether the observed anomalies support the concept of an active passive margin, as previously proposed in global tectonic studies.

3.1 Electromagnetic environment

The electromagnetic (EM) environment of the research area presents unique challenges for MT surveys due to extensive human activities and diverse natural and artificial noise sources. The region's high population density, industrial infrastructure, and aquaculture operations contribute to significant EM interference, necessitating careful site selection and rigorous data processing to extract reliable geophysical signals.

Despite efforts to position MT stations in remote locations, anthropogenic noise remains prevalent. High-voltage power lines, communication towers, and industrial machinery generate strong EM fields that can obscure natural telluric signals. Additionally, aquaculture systems near the Pearl River Delta estuary introduce periodic electrical noise from aeration systems and water pumps, affecting stations such as ZHMT04A to ZHMT07A. Small-scale factories with irregular operating schedules further contribute to unpredictable EM contamination, complicating data acquisition and requiring robust noise mitigation techniques.

To evaluate the impact of these noise sources, spectral analysis of the raw time-series data was performed. The results indicate that:

- Power-line interference is dominant at 50 Hz and its harmonics, with varying intensity depending on proximity to infrastructure.
- Localized industrial sources introduce narrowband noise at 15-40 Hz, detected at stations near urbanized areas.

https://doi.org/10.5194/egusphere-2025-2073
Preprint. Discussion started: 18 June 2025

- Transient, non-periodic spikes were observed in several stations, likely linked to intermittent electrical discharges from industrial equipment.

The severity of noise contamination varied by location and time of day. Based on time-series analysis, the quietest data windows typically occurred between 1:00 AM and 5:00 AM, suggesting that future surveys in similar environments could benefit from prioritizing night-time data acquisition and utilizing extended recording duration to improve data stacking and noise suppression.

While electromagnetic interference posed challenges, the robust data selection and processing strategies employed in this study ensured that decent-quality impedance estimates were obtained for inversion.

3.2 Electrical structure of the research area

The inverted resistivity model derived from the MT survey along the research area reveals significant conductivity variations that correlate with key geological features. Unlike a simple layered resistivity structure, the model exhibits complex lateral and vertical resistivity contrasts, indicating the presence of multiple geological units, fault zones, and deep-seated anomalies. The resistivity model extends to a depth of 20 km, covering the crustal structure from the near-surface layers to the Moho transition.

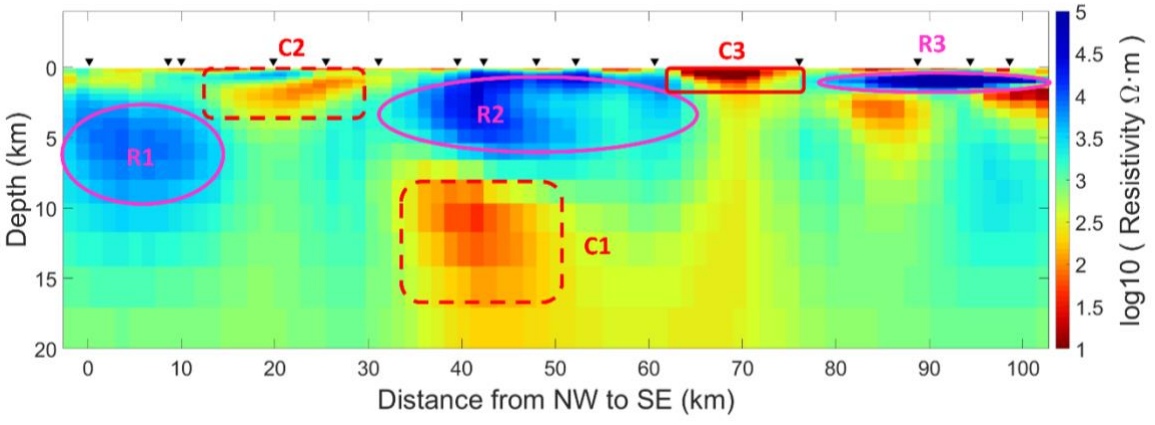

Figure 8: Identified anomalies in the resistivity model along the ZHMT survey transect (with ocean and sediment in initial model), highlighting key geological features and potential subsurface structures.

Figure 8 presents the resistivity distribution along the survey line, highlighting several notable anomalies. These features were identified based on resistivity contrasts, structural patterns, and their correlation with known geological constraints. The six primary anomalies are:

- C1 Deep low-resistivity anomaly beneath Shuangshui and Luokeng Township, Xinhui District (SLRA): This anomaly, extending from 10 km to 15 km depth, represents the most significant deep crustal conductor in the model. It coincides with a previously reported low-velocity zone from seismic survey (Lü et al., 2022), suggesting a possible connection between resistivity and seismic velocity reductions.

https://doi.org/10.5194/egusphere-2025-2073
Preprint. Discussion started: 18 June 2025

- C2 Northwest-dipping conductive structure: Located at the western section of the profile, this feature is interpreted as a concealed fault zone that facilitates fluid infiltration, lowering the bulk resistivity. Geological maps suggest the presence of a deep-seated fault, which aligns with this conductivity anomaly. Furthermore, seismic data (Lü et al., 2022) also complement the identification of such hidden fault with the presence of a low-velocity anomaly at the same location.
- C3 Shallow low-resistivity anomaly near the Pearl River estuary: This anomaly corresponds to the highly conductive sediments and water-saturated deposits in the deltaic region, where marine and fluvial processes have accumulated thick layers of unconsolidated material.
- R1, R2, R3 Resistive zones associated with intrusive granite: Several high-resistivity regions correspond to known granite intrusions that form part of the regional basement. These intrusive bodies, identified in geological surveys, exhibit significantly higher resistivity than surrounding environments.

To further investigate the depth extent and nature of these anomalies, a horizontal slice of the resistivity model at 10 km depth is shown in Figure 9. The distribution of conductive and resistive regions at this depth highlights the complex framework of the research region, with conductive zones aligning with possible fluid-bearing structures. The 3D resistivity model values distant from the survey line are less controlled by the data and more sensitive to the initial and reference model of the inversion.

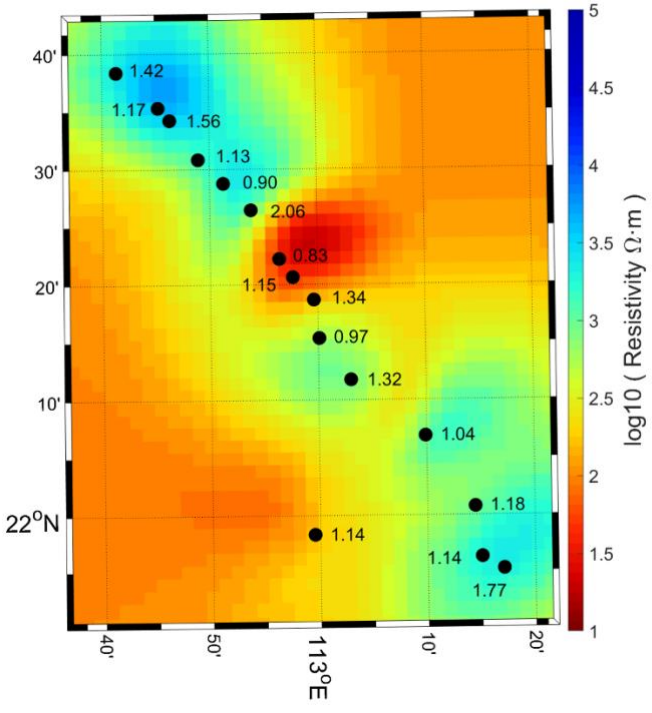

Figure 9: Resistivity model from inversion (plan view) at depth = 10 km. The number next to each station dot represents the rms of each station.

https://doi.org/10.5194/egusphere-2025-2073
Preprint. Discussion started: 18 June 2025

Overall, the resistivity model provides new constraints on the subsurface architecture of the research region, refining our understanding of crustal deformation, fluid distribution, and lithospheric heterogeneity in this passive margin setting. These findings serve as a foundation for further geodynamic interpretation, which are discussed in the following section.

3.3 Geological and tectonic insight

The resistivity model not only aligns with known geologic and geographic features—such as the Pearl River estuary and regional fault structure—but also reveals a previously unrecognized deep conductive anomaly beneath Shuangshui and Luokeng Town, Xinhui District. This Shuangshui low-resistivity anomaly (SLRA), located at 10-15 km depth, stands out as the most significant deep crustal feature in the study area. Its presence suggests an underlying geodynamic process distinct from the surrounding resistive crust.

Notably, SLRA coincides with a low-velocity zone identified in seismic studies (Lü et al., 2022; Cao et al., 2014), indicating a weakened crustal region potentially linked to fluid accumulation, partial melting, or other tectonic processes. Given its depth and conductivity characteristics, this anomaly may represent a shear zone or deep-seated fault structure facilitating fluid migration, a feature often observed in tectonically active passive margins.

To explore its geological significance, this section investigates two possible origins for SLRA:

- A fluid-bearing shear zone, where extensive faulting has led to localized fluid enrichment, reducing both resistivity and seismic velocity.
- Partial melting of mid-crustal material, which would imply an anomalous thermal structure or residual mantle influence in the region.

Through this analysis, we assess whether the presence of such a deep conductive anomaly challenges the conventional perception of the research region as a purely passive margin, instead hinting at more complex geodynamic interactions.

3.3.1 Fluid-bearing Shear Zone

The Shuangshui low-resistivity anomaly (SLRA), observed at depths of 10-15 km, is interpreted as a fluid-bearing shear zone. This anomaly, characterized by significantly lower resistivity and seismic velocity, suggests the presence of a deep-seated fault system that acts as a conduit for fluid migration. The region's extensional tectonic history, specifically during the seafloor spreading phase of the South China Sea, likely contributed to the development of such fault zones, which are typical pathways for fluids generated by magmatic or metamorphic processes.

The S-wave velocity (Vs) drop, from 3.75 km/s to 3.5 km/s, within the anomaly aligns with what is typically observed in fluid-saturated shear zones. Studies indicate that a 2-5% fluid volume fraction in the crust can result in a 6-8% reduction in Vs, as the presence of fluids in pore spaces and fractures weakens the rock matrix, reducing its seismic velocity (Watanabe, 1993; Shelly et al., 2015).

The observed seismic velocity reduction and the associated resistivity decrease are consistent with the behaviour of shear zones that have been enriched by fluids, which can cause brittle-ductile transitions and facilitate fault reactivation.

https://doi.org/10.5194/egusphere-2025-2073
Preprint. Discussion started: 18 June 2025

The low-resistivity anomaly observed in the Shuangshui region further supports this interpretation. Fluids within the shear zone would enhance charge transport, significantly reducing resistivity. This is particularly evident in the depth range of 10-15 km, where the resistivity is markedly lower than the surrounding crust. These findings suggest that the fluid accumulation in this shear zone is likely not a transient feature but a stable and potentially active geological structure that has been sustained over time.

While the exact composition of the fluids remains uncertain, their role in weakening the crust is likely significant. Fluid migration through the shear zone may not only influence the local resistivity and seismic velocity but could also impact the region's seismic behaviour. The presence of such a fluid-rich shear zone may contribute to stress transfer and fault reactivation, which could explain the recent small earthquakes (Mw 3-4) observed in the research region. These seismic events align with the notion of an active passive margin, where underlying fault zones, typically considered dormant in a passive margin setting, are reactivated due to the presence of fluids. This challenges the conventional perception of the research region as a purely stable passive margin and suggest more complex geodynamic interactions at play.

The presence of this fluid-bearing shear zone also has implications for regional geothermal activity. Fluids migrating through deep crustal fault zones can facilitate magmatic intrusions or hydrothermal circulation, both of which contribute to increase heat flow. Given the observed elevated surface heat flow in the region (Kuang et al., 2021), it is plausible that the fluid-rich shear zone may play a role in the region's thermal evolution, further influencing both seismic activity and crustal deformation.

3.3.2 Partial Melting of Mid-crustal Material

Another plausible explanation for SLRA is partial melting of mid-crustal material, which could be the result of magmatic activity or elevated geothermal gradients in the region. The elevated surface heat flow in the region, measured at 70-90 mW/m^2 (Kuang et al., 2021), provides compelling evidence for anomalous thermal conditions that could induce partial melting in the lower crust. This heat flow is higher than the regional average for passive margins, which typically ranges between 40-60 mW/m^2, supporting the hypothesis of anomalous magmatic or mantle-related activity beneath the research region.

Partial melting at mid-crustal depths typically results in a decrease in seismic velocity and resistivity, similar to what is observed in SLRA. Melted materials, such as basaltic or granitic partial melts, exhibit significantly lower resistivity due to the presence of conductive melt phases, which increase the electrical conductivity of the crust. As a result, the low resistivity observed in the anomaly could represent partial melts within the crust-mantle transition zone, or localized areas of higher porosity, potentially linked to crustal extension or fluid migration.

The seismic velocity reduction from 3.75 km/s to 3.5 km/s, as observed in the Shuangshui region, is consistent with the velocity changes expected in the regions of 3-5% of partial melting (Takei, 2002; Hammond and Humphreys, 2000). The presence of melt within the crust typically leads to lower seismic velocities in comparison to surrounding rock, due to the lower rigidity of melt-bearing rocks.

https://doi.org/10.5194/egusphere-2025-2073
Preprint. Discussion started: 18 June 2025

Additionally, the presence of high heat flow in the region could promote magmatic intrusions that contribute to both crustal deformation and further thermal anomalies. The proximity of SLRA to the LFZ also suggests that fault-related processes may play a role in initiating partial melting by providing fluid pathways and localized heating zones at depth. These factors, combined with the observed geophysical anomalies, imply a potential thermos-mechanical coupling between magmatic processes and extensional faulting in the region.

4 Conclusion

This study highlights the complexity of the continental edge near the northern part of the South China Sea revealed through MT data, which uncovers significant electrical anomalies that challenge the conventional perception of the region as a passive margin. The Shuangshui low-resistivity anomaly (SLRA) at the depth of 8-15 km stands out as the most striking feature overlapping with a low shear-wave velocity zone. We propose two possible interpretations: a fluid-bearing shear zone or a region of partial melting. Both interpretations suggest an active geodynamic process in the mid-crust beneath what was once thought to be a stable, passive margin.

However, the conclusions drawn from this study are based on a limited dataset, and further investigation is required to fully understand the geodynamic processes driving these anomalies. To refine the resistivity model and strengthen our understanding, additional MT data, including higher-resolution meshing and more seismic data (such as Vp/Vs ratios), would provide crucial insights into subsurface structures. Moreover, geothermal data could offer essential constraints on heat flow and thermal gradients, helping to differentiate between fluid-bearing processes and partial melting.

Future research that integrates MT data, seismic velocities, and geothermal measurements will be instrumental in clarifying the geodynamic processes at play in the research region. Such a comprehensive dataset will allow for more accurate models, shedding light on the tectonic evolution of the region and improving our understanding of the seismic hazards associated with active passive margins.

5 Author Contribution

S.F. acquired and processed the magnetotelluric data, conducted the resistivity inversion, performed the geological and geophysical interpretation, and wrote the manuscript.

D.Y. designed and supervised the project, provided funding, and contributed to the manuscript revisions.

F.J. participated in the data acquisition process, provided scientific consultation and assisted with manuscript revisions.

C.Y. advised on the seismic literature and contributed interpretative insights.

X.L. conducted the literature review on seismic studies and prepared Fig.2 based on published data.

https://doi.org/10.5194/egusphere-2025-2073
Preprint. Discussion started: 18 June 2025

6 Acknowledgement

This project was supported by Southern Marine Science and Engineering Guangdong Laboratory (Zhuhai) (No. SML2021SP303), Guangdong Provincial Key Laboratory of Geophysical High-resolution Imaging Technology (2022B1212010002), Centre for Computational Science and Engineering of Southern university of Science and Technology. The authors thank Lü et al. (2022) for providing their velocity model. Yangtze University helped with the field data acquisition. Dr. Peijing Wang helped with the MTDP software.

References

Armitage, J., Jaupart, J.J., Fourel, L., and Allen, P.A.: The instability of continental passive margins and its effect on continental topography and heat flow, J. Geophys. Res. Solid Earth, 118, 1817-1836, doi: 10.1002/jgrb.50097, 2013.

Bao, Y., Lu, J., Li, X., Zhang, X., Chen, D., Wang J., Luo, Y., and Chen, Z.: Source current mechanism of the daily ratio of geomagnetism before the M_L4.6 earthquake in Huidong, Guangdong province, Progress in Geophysics, 39(4), 1358-1368, doi: 10.6038/pg2024HH0095, 2024.

Buck, W.R.: 6.08 – The Dynamics of Continental Breakup and Extension, Treatise on Geophysics (Second Edition), Elsevier, 325-379, ISBN 9780444538031, doi: 10.1016/B978-0-444-53802-4.00118-4, 2015.

Cai, W., Li, J., and Xiao, C.: Geothermal power generation and positive impact in the greater bay area: a case study of Huizhou City, Guangdong Province, Sci Rep 14, 4095, doi: 10.1038/s41598-024-53738-1, 2024.

Cao, J., Xia, X., Sun, J., Zhu, J., Xu, H.: Preliminary results of onshore-offshore seismic experiments in a potential strong earthquake area off the Pearl River Estuary, Journal of Tropical Oceanography (Chinese), 31(3), 71, doi: 10.3969/j.issn.1009-5470.2012.03.010, 2012.

Cao, J., Sun, J., Xu, H., Xia, S.: Seismological features of the littoral fault zone in the Pearl River Estuary, Chinese Journal of Geophysics (Chinese), 57(2), 498, doi: 10.6038/cjg20140215, 2014.

Ebinger, C., Belachew, M.: Active passive margins, Nature Geoscience 3, 670-671, doi:10.1038/ngeo972, 2010.

Hammond, J.O.S. and Humphreys, E.D.: Upper mantle seismic wave velocity: Effects of realistic partial melt geometries, Journal of Geophysical Research: Solid Earth, 105(B5), 10975-10986, doi:10.1029/2000JB900041, 2000

Huang, H., Klingelhoefer, F., Qiu, X., Li, Y., Wang, P.: Seismic imaging of an intracrustal deformation in the northwestern margin of the South China Sea: The role of a ductile layer in the crust, Tectonics, 40, e2020TC006260, doi: 10.1029/2020TC006260, 2021.

Huang, J., Wang, Y., and Guo, L.: Energy intensity and energy-specific technological progress: A case study in Guangdong province of China, Renewable Energy, 184, 990-1001, doi: 10.1016/j.renene.2021.11.087, 2022.

https://doi.org/10.5194/egusphere-2025-2073
Preprint. Discussion started: 18 June 2025

Huang, R., Deng, Y., Chen, Y., Xiong, C., Zhang, Z.: Source parameters and stress triggering of 2023 M⩾4 earthquakes sequence in Heyuan, Guangdong, Chinese Journal of Geophysics (Chinese), 68(3): 956-969, doi: 10.6038/cjg2024R0701, 2023.

Kang, Y., Yang, X., Chen, X. et al.: Inversion of stress field in Guangdong and its adjacent area, Acta Seismol. Sin. 21, 58-66, doi:10.1007/s11589-008-0058-y, 2008.

Kirby, A.L., Zhang, F., Peacock, J., Hassan, R., Duan, J.: The MTPy software package for Magnetotelluric data analysis and visualization, Journal of Open Source Software, 4(37), 1358, doi: 10.21105/joss.01358, 2019.

Kuang, J., Qi, S., and Hu, X.: New Insights into Crust and upper Mantle Structure in Guangdong Province, China and Its Geothermal Implications, Energies, 14(8), 2236, doi:10.3390/en14082236, 2021.

Li, F., Huan, W.: Quaternary Activity Characteristics of the Coastal Fault Zone in Eastern Guangdong, Technology for Earthquake Disaster Prevention (Chinese), 16(1), 19, doi:10.11899/zzfy20210103, 2021.

Lü, Z., Huang, H., Ye, X., Lv, J., and Xiong, C.: High-Resolution Crustal Shear-Wave Velocity Structure in the Pearl River Delta, South China, Seismol. Res. Lett. 93(1), 338-350, doi: 10.1785/0220210116, 2022.

Meju, M.A., Gallardo, L.A., Mohamed, A.K.: Evidence for correlation of electrical resistivity and seismic velocity in heterogenous near-surface materials, Geophysical Research Letters, doi: 10.1029/2002GL016048, 2003.

Moorkamp, M., Roberts, A.W., Jegen, M, Heincke, B., Hobbs, R.W.: Verification of velocity-resistivity relationships derived from structural joint inversion with borehole data, Geophysical Research Letters, doi: 10.1002/grl.50696, 2013.

Pallister, J., McCausland, W., Jonsson, S. et al.: Broad accommodation of rift-related extension recorded by dyke intrusion in Saudi Arabia, Nature Geoscience 3, 705-712, doi: 10.1038/ngeo966, 2010.

Ruan, A., Wei, X., Niu, X., Zhang, J., Dong, C., Wu, Z., Wang, X.: Crustal structure and fracture zone in the Central Basin of the South China Sea from side angle seismic experiments using OBS, Tectonophysics, 688(1), 10, 2016.

Satyakumar, A.V., Jin, S., M.Tiwari, V., Xuan, S.: Crustal structure and isostatic compensation beneath the South China Sea using satellite gravity data and its implications for the rifting and magmatic activities, Physics of the Earth and Planetary Interiors, 344, 107107, doi: 10.1016/j.pepi.2023.107107, 2023.

Shelly, D.R., Taira, T.A, Prejean, S.G., Hill, D.P. and Dreger, D.S.: Fluid-faulting interactions: Fracture-mesh and fault-valve behaviour in the February 2014 Mammoth Mountain, California, earthquake swarm, Geophysical Research Letters, 42(14), 5803-5812, doi:10.1002/2015GL064325, 2015.

Takei, Y.: Effect of pore geometry on VP/VS: From equilibrium geometry to crack, Journal of Geophysical Research: Solid Earth, 107(B2), doi: 10.1029/2001JB000522, 2002

Wang, Y., Lin, W., Xi, Y.: Heat Flow Distribution in the Continental Area of China Based on the Relationship between Geologic Age and Heat Flow, Earth Science-Journal of China University of Geosciences, doi: 10.3799/dqkx.2022.384, 2022.

Wang, L., Zhang, Y., Wang, W., Liu, S., Ye, X., Yang, W., Xu, S., Ma, X.: Three-dimensional shallow velocity structure beneath the central area of Guangdong-Hong Kong-Macao Greater Bay Area revealed by methane source and dense array, Chinese Journal of Geophysics (Chinese), 66(11), 4582, doi: 10.6038/cjg2022Q0702, 2023.

https://doi.org/10.5194/egusphere-2025-2073
Preprint. Discussion started: 18 June 2025

Wang, P., Chen, X., Han, P., et al.: Strong interference Magnetotelluric data processing method based on robust estimation, data screening and Rhoplus constraint, Chinese J. Geophys. (Chinese), 67(11): 4325-4342, doi: 10.6038/cjg2024R0839, 2024.

Watanabe, T.: Effects of water and melt on seismic velocities and their application to characterization of seismic reflectors, Geophysical Research Letters, 20(24), 2933-2936, doi: 10.1029/93GL03170, 1993.

Wu, K., He, L., Guo, Z., Luo, B., Chen, Y.J., and Osotuyi, A.G.: Upper crustal structure of the Xinfengjiang reservoir from ambient noise double beamforming tomography and its implications for induced seismicity, Geophysical Journal International, 240(2), doi:10.1093/gji/ggae427, 2024.

Xiong, C., Cao, J., Sun, J., Xia, S., Wan, K., Fan, C., Yang B.: Variation Characteristics along the Strike of the Littoral Fault Zone in Offshore Pearl River Estuary, Earth Science (Chinese), 43(10), 3682, doi: 10.3799/dqkx.2018.553, 2018.

Ye, X., Wang, L., Xiong, C., Lu, Z., Wu, H.: Introduction to the project of shallow three-dimensional crustal structure exploration (Phase I) in Guangdong – Hong Kong – Macao Greater Bay Area, Seismological and Geomagnetic Observation and Research (Chinese), 43(Suppl1), 28, doi: 10.3969/j.issn.1003-3246.2022.S1.009, 2022.

Yeh, Y., Hsu, S., Doo, W., Sibuet, J., Liu, C., Lee, C.: Crustal features of the northeastern South China Sea: insights from seismic and magnetic interpretations, Mar Geophys Res, 33:307-326, doi: 10.1007/s11001-012-9154-4, 2012.

Zhang Y., Ye, X., Wan, K., Lv, Z., Wen, G., Xu, S.: Fault structure, seismicity, and magnetism of the Littoral Fault zone, northern South China Sea: Insights from high-resolution seismic reflection data, Marine and Petroleum Geology, 160, 106605, doi: 10.1016/j.marpetgeo.2023.106605, 2024.